ADVANCED MATERIALS
www.advmat.de

# Bio-Inspired Multiple Responsive NIR II Nanophosphors for Reversible and Environment-Interactive Information Encryption

*Tianpei He, Jing Xi, Rui Zhao, Na Chen,* and Quan Yuan**

**Inspired by the natural responsive phenomena, herein the multiple responsive persistent luminescent $Zn_{1.2}Ga_{1.6}Ge_{0.2}O_4:Ni^{2+}$ (ZGGO:Ni) nanoparticles with near-infrared (NIR) II emission peak ≈1330 nm derived from the $Ni^{2+}$ doping through controlled synthesis based on hydrothermal method are obtained. The obtained NIR II persistent luminescent ZGGO:Ni can not only respond to temperature but also the specific solvent stimulus. The results demonstrate that the NIR II persistent luminescence intensity decreases in hydroxyl containing solvent such as water ($H_2O$) and ethyl alcohol ($C_2H_6O$), while the PL intensity remains in solvent without hydroxyl groups such as n-hexane ($C_6H_{14}$) and deuterated water ($D_2O$). This NIR II luminescence quenching is attributed to the adsorption of interaction hydroxyl groups in specific solvents with the amino group on the surface of ZGGO:Ni and the subsequent fluorescence resonance energy transfer mechanism. Benefiting from the multiple responsive properties, the obtained NIR II persistent luminescent ZGGO:Ni is utilized for high-order dynamic optical information encryption, providing increased security level. The multi-responsive NIR II persistent luminescence strategy outlined in this study is anticipated to offer a straightforward methodology for optimizing the optical characteristics of NIR II persistent luminescent materials. Moreover, it is set to expand the scope of their applications in the realm of dynamic and environment-interactive information encryption, thereby opening frontiers for their utilization in advanced security measures.**

## 1. Introduction

In nature, many organisms have evolved the ability ingeniously to interact with the external environment, equipping themselves to avoid damage from an outside force and to increase their survival.[1] For example, the well-known chameleons are capable to dynamically change their color appearance through the variation of the guanine nanocrystal structures beneath their skin in response to external environment, enabling self-camouflage and species warning communications.[2] Recently, inspired by the natural responsive phenomena, responsive nanomaterials that can respond to various external stimuli such as light, heat and humidity into signals have raised numerous attentions and have been widely adopted in the application of biosensing, information encryption, smart home and etc.[3] However, the currently reported responsive nanomaterials are largely limited and most of them can only realize a single stimulus-response such as temperature,[4] humidity,[5] pH.[6] Additionally, the responsive mechanism of nanomaterials are still remaining unclear, limiting the design and development of responsive nanomaterials with multi-functions for intelligent biosensing, information encryption and etc.

Persistent luminescent nanomaterials, which enables the storage of photogenerated charge carriers through the defect structures, can remain the luminescence even after the excitation ceases under the external stimulation.[7] The defect structures and electronic structures of persistent luminescent nanomaterials can be dynamically regulated in respond to the external environment such as heat and light, thus achieving the dynamic and multiple responses.[8] The intrinsic above optical properties of persistent luminescent nanomaterials are well suited for the design and exploit of new external stimulus responsive nanomaterials. Near-infrared (NIR) II nanomaterials (ranging from 1000 to 1700 nm) with the unique advantages such as strong concealment, resistance to visible light interference, and deep tissue penetration, have recently garnered significant attention.[9] Developing NIR II persistent luminescent nanomaterial with multiple and sensitive responses to external stimulus is crucial for

T. He, J. Xi, R. Zhao, N. Chen, Q. Yuan
College of Chemistry and Molecular Sciences
Renmin Hospital of Wuhan University
Institute of Molecular Medicine
School of Microelectronics
Wuhan University
Wuhan 430072, P. R. China
E-mail: chenna0804@whu.edu.cn; yuanquan@whu.edu.cn
Q. Yuan
Molecular Science and Biomedicine Laboratory (MBL)
State Key Laboratory of Chemo/Biosensing and Chemometrics College of Chemistry and Chemical Engineering
Hunan University
Changsha 410082, P. R. China

The ORCID identification number(s) for the author(s) of this article can be found under https://doi.org/10.1002/adma.202416399

DOI: 10.1002/adma.202416399

 

the facilitated development in smart biosensing, bioimaging, and information encryption. Unlocking the synthesis of NIR II persistent luminescent nanomaterials and delineating the response mechanisms are essential for achieving sensitive and dynamically responsive materials to external stimuli, offering tools and insights to broaden their potential applications.

Inspired by the natural phenomenon in which chameleons camouflage themselves in response to external environmental factors, herein we obtained the multiple responsive NIR II persistent luminescent $Zn_{1.2}Ga_{1.6}Ge_{0.2}O_4:Ni^{2+}$ (ZGGO:Ni) peaked ≈1330 nm through controlled synthesis based on hydrothermal method for environment-interactive information encryption applications. According to the structure-activity relationship analysis, it is found that the NIR II emission derives from the $Ni^{2+}$ doping by introducing new energy levels. Additionally, the obtained NIR II persistent luminescent ZGGO:Ni can not only respond to temperature but also the solvent stimulus. The results demonstrate that the NIR II persistent luminescence (PL) intensity decreases in hydroxyl solvent such as water ($H_2O$) and ethyl alcohol ($C_2H_6O$), while the PL intensity remains in solvent without hydroxyl groups such as n-hexane ($C_6H_{14}$) and deuterated water ($D_2O$). Based on the results and the previous reports, it is hypothesized that the NIR II PL responses to the external solvent owing to the adsorption of interaction groups in specific solvents with the amino group on the surface of ZGGO:Ni and the subsequent fluorescence resonance energy transfer mechanism. Moreover, the obtained multiple responsive NIR II persistent luminescent ZGGO:Ni has been utilized for multi-color and dynamic optical information encryption to further increase the security level as demonstrated in **Figure 1**. Overall, the proposed multiple responsive NIR II PL strategy in this work is expected to provide a facile method for the optical properties optimization of NIR II persistent luminescent materials and pave ways for broadening their applications in multi-dimensional and dynamic information encryption (**Scheme 1**).

## 2. Results and Discussion

### 2.1. Preparation and Environmental Responsiveness of NIR II ZGGO:Ni Nanophosphor

Currently, a serious NIR II nanophosphors have been developed such as $NaYF_4$:Ln@$NaYF_4$,[10a] $Cs_2M(Ln_{1-x}Sb_x)Cl_6$ (M = alkali metal),[10b] $CaSnO_3$,[10c] $MgGeO_3$:Ln,[10d] and etc.[10e,f] However, researchers mainly focus on the bioimaging application in deep tissue and there is a scarcity of studies exploring the NIR II persistent luminescence responses to environmental stimuli.[9h] Zinc gallogermanate (ZnGaGeO) has garnered significant interest in the development of phosphor materials owing to its facile synthesis process and outstanding performance characteristics.[11] $Ni^{2+}$ has been previously recognized for its octahedral coordination, which enables d-d electronic transitions. These specific valence substitutions play a crucial role in generating persistent luminescence within the near-infrared (NIR) II region.[12,13] Indeed, numerous studies have focused on developing innovative NIR II persistent luminescent materials centered around $Ni^{2+}$.[13] However, most of the materials documented to date have bulky architectures,[13] which inherently limits their wider application prospects. Moreover, the multi-responsive properties and environment-interactive functionalities of these NIR II persistent luminescent materials remain largely uncharted territories.[14]

Herein, we obtained the NIR II long afterglow nanophosphor ZGGO:Ni by a hydrothermal method (Figure S1, Supporting Information). As shown in Figure 1a, the prepared nanophosphors can remain the NIR II luminescence even after the excitation ceases. It can be observed that the synthesized ZGGO:Ni samples predominantly exhibit a spherical morphology with uniform shapes and sizes, distributed within a range of 10 to 25 nm (Figure 1b; Figure S2, Supporting Information). The X-ray diffraction (XRD) pattern of ZGGO: Ni (Figure S3, Supporting Information) reveals diffraction peaks consistent with the standard pattern of JCPDS 38–1240, indicating a typical cubic spinel structure. In addition, as shown in Figure S4 (Supporting Information), it can be observed that all elements including Zn, Ga, Ge, O, and Ni are uniformly distributed across the surface and interior of nanoparticles, indicating the successful introduction of $Ni^{2+}$ ions into ZGGO.

Subsequently, the optical properties and responsive behaviors are further explored. According to the transient decay curve in Figure 1c, the photogenerated electron lifetime of ZGGO: Ni can be calculated to be 190.3 µs, suggesting a long lifetime persistent luminescence. Furthermore, the introduction of $H_2O$ onto the surface of ZGGO:Ni nanoparticles results in a noticeable reduction in the lifetime of photogenerated electrons, signifying the occurrence of a quenching effect. Additionally, it can also be seen clearly that the persistent luminescence intensities in visible and NIR regions with the peaks ≈410 and 1330 nm both decreased dramatically upon the addition of $H_2O$ as demonstrated in Figure 1d,e, further validating that $H_2O$ or humility impacts on the optical properties of the NIR II persistent luminescent ZGGO: Ni nanoparticles. The NIR II decay images shown in Figure 1f illustrate that the ZGGO:Ni phosphors are capable of emitting persistent NIR II luminescence even after excitation ceases, a property that lasts for up to 800 ms. However, upon the introduction of $H_2O$, the persistent NIR II luminescence is effectively quenched (Figure 1g). Considering that phosphor materials can typically response to external stimulus such as temperature as reported previously,[15] the NIR II decay images at different temperatures have also been obtained. As illustrated in Figure 1h, it is evident that the intensity of NIR II persistent luminescence diminishes with the rise in temperature. This reduction can be attributed to the enhanced release of trapped carriers, which promotes recombination luminescence (Figure 1i). Above all, the aforementioned findings demonstrate that the prepared NIR II persistent luminescent ZGGO:Ni nanoparticles exhibit responsive optical properties to both $H_2O$ and temperature variations. The prepared NIR II ZGGO:Ni nanophosphor, endowed with the unique environmental responsiveness, is poised to outperform alternative nanophosphors in the realms of intelligent sensing and environment-interactive information encryption.

### 2.2. Mechanisms of the NIR II Persistent Luminescence and the Environmental Responsiveness

To gain profound insights into the NIR II persistent luminescence mechanism and the responsiveness of the prepared ZGGO:Ni nanophosphors, further investigations into the

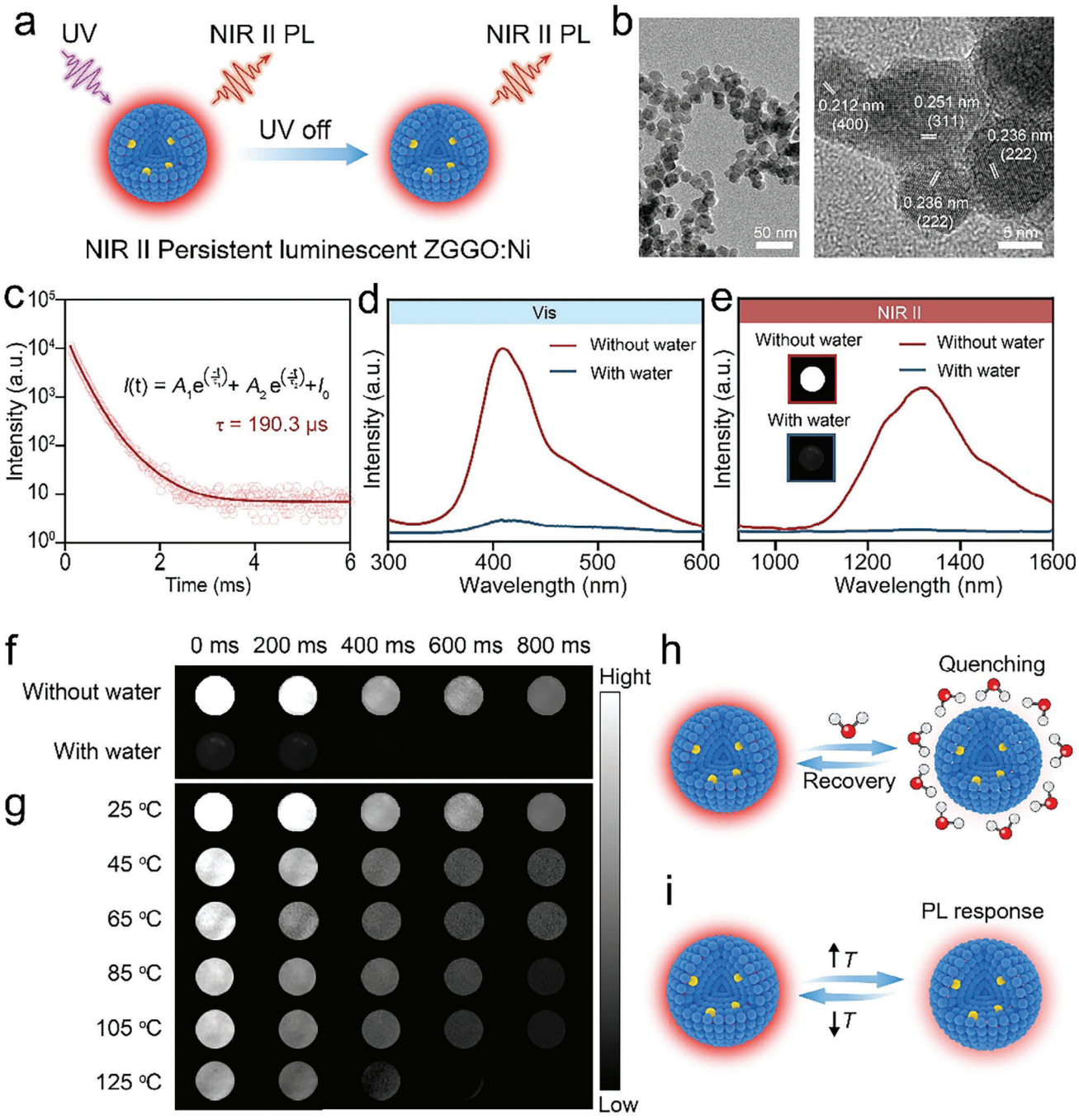


**Figure 1.** Characterization of the structure and optical properties of ZGGO:Ni nanophosphor. (a) Schematic illustration of the ZGGO:Ni nanophosphor with NIR II emission. (b) TEM image of ZGGO: Ni. (c) transient decay curves of ZGGO: Ni. (d) Persistent luminescence spectra of ZGGO: Ni in visible region under 275 nm excitation. (e) Persistent luminescence spectra of ZGGO:Ni in NIR region under 275 nm excitation. (f) NIR persistent luminescence decay images upon the addition of water across time. (g) Schematic illustration of the NIR persistent luminescence quenching of ZGGO:Ni nanophosphor. (h) NIR persistent luminescence decay images under different temperature conditions. (i) Schematic illustration of the NIR persistent luminescence response to environmental temperature variations.

electronic and defect structures, as well as the energy transfer processes were conducted. The phosphorescence spectrum presented in **Figure** 2a clearly indicates that the NIR peak emission centered ≈1330 nm is a distinctive feature of ZGGO:Ni nanophosphors, whereas the ZGGO nanophosphor does not exhibit NIR emission characteristics. In addition, it can be found that the emission intensity peaked ≈410 nm in visible region both in ZGGO and ZGGO:Ni, which can be ascribed to ZGGO host material (Figure S5, Supporting Information). These observations strongly suggest that the presence of $Ni^{2+}$ doping is

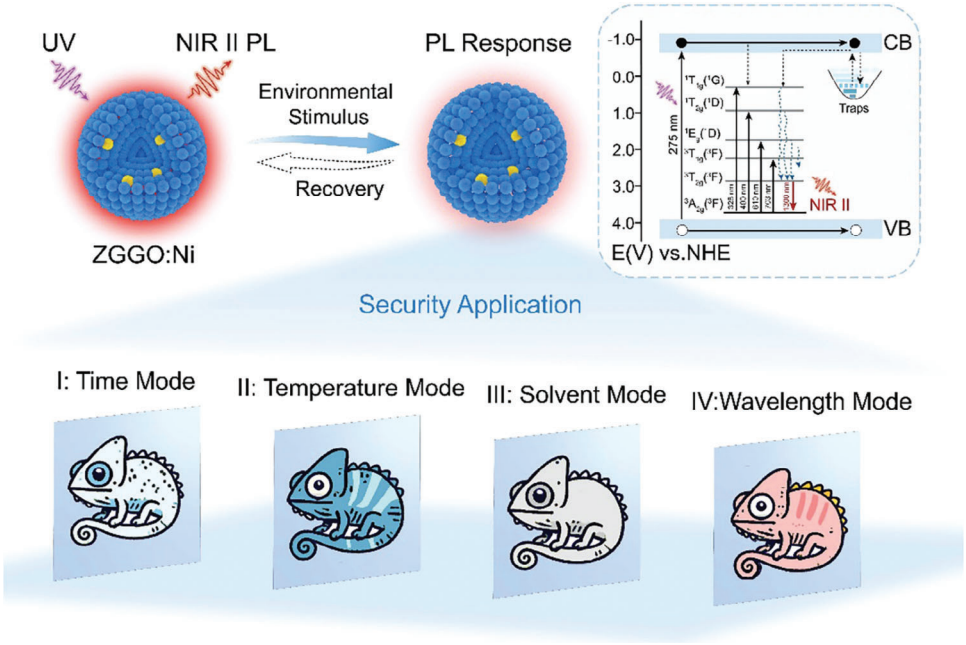


**Scheme 1.** Schematic illustration of the NIR II persistent phosphors for multiple and dynamic information encryption.

directly linked to the NIR II emission phenomenon. Furthermore, it is noticeable that the NIR II emission intensity initially increases with the rising concentration of $Ni^{2+}$ and subsequently declines. The doping contents of $Ni^{2+}$ were further tested with inductively coupled plasma mass spectrometry (ICP-MS) (Table S1, Supporting Information). The results indicate that excess $Ni^{2+}$ doping leads to a decrease in luminescence efficiency, which can be ascribed to the concentration quenching effects (Figures S6 and S7, Supporting Information).[16] Furthermore, the ZGGO:Ni nanophosphors demonstrate a significant NIR II emission with a high quantum yield of 12.3%, which is comparable to previously reported NIR phosphors.[9i,11d] The Tauc plot depicted in Figure 2b reveals that the bandgap of the ZGGO:Ni nanophosphor is 4.36 eV. The photoelectron spectroscopy (UPS) spectrum as shown in Figure 2c,d enables us to determine that the Fermi level ($E_{fermi}$) is located at 3.58 eV, while the cutoff energy ($E_{cutoff}$) is positioned at 16.34 eV. Subsequently, the valence band edge ($E_{VB}$) has been calculated to be −8.46 eV with the detailed methodology provided in the methods section. Consequently, the conduction band ($E_{CB}$) edge potential can be calculated to be located at −0.40 V. The excitation spectrum in Figure 2e demonstrates four excitation peaks which can be ascribed to $^3A_{2g}(^3F)$—$^1E_g(^1G)$, $^3A_{2g}(^3F)$—$^3T_{1g}(^3P)$, $^3A_{2g}(^3F)$—$^1E_g(^1D)$ and $^3A_{2g}(^3F)$—$^3T_{1g}(^3F)$.[17] Additionally, according to the thermoluminescence spectra of NIR II ZGGO:Ni nanophosphor, the trap depths $E$ (with respect to the conduction band edge) can be roughly estimated to be 0.75 eV, which is recognized to be a good compromise for a strong room temperature long-lasting luminescence (Figure S8, Supporting Information). Based on the measured emission spectrum, the excitation spectrum, and the determined bandgap value, the NIR II persistent luminescence mechanism for the prepared NIR II ZGGO nanophosphor has been proposed. As shown in Figure 2f, the $Ni^{2+}$ doping introduces new energy levels and the NIR II persistent luminescence at 1330 nm can be ascribed to the defect trapped charge transfer transitions $^3T_{2g}(^3F)$—$^3A_{2g}(^3F)$.[17]

As previously discussed, our findings reveal that the prepared NIR II persistent luminescent ZGGO:Ni nanoparticles exhibit responsiveness to external $H_2O$. To delve deeper into the underlying responsive mechanisms, we have expanded our investigation to include the nanophosphor's reactivity to a variety of molecules, such as dimethyl sulfoxide ($C_2H_6OS$), tetrahydrofuran ($C_4H_8O$), n-hexane ($C_6H_{14}$), acetonitrile ($C_2H_3N$), ethyl alcohol ($C_2H_5OH$), methyl alcohol ($CH_3OH$) and deuterated water ($D_2O$). As evidenced in the decay images captured in the near-infrared (NIR) region in Figure 2g and the persistent intensities in the NIR II window in Figure 2h, it is interesting to find that the addition of $C_2H_6OS$, $C_4H_8O$, $C_6H_{14}$, $C_2H_3N$ or $D_2O$ does not significantly alter the decay intensities of the ZGGO:Ni nanophosphors. The persistent luminescence intensities all remain comparable to those of the unadulterated ZGGO:Ni over time. In contrast, the luminescence intensities of the ZGGO:Ni nanophosphors are evidently diminished with the introduction of $C_2H_5OH$, $CH_3OH$, and $H_2O$. Additionally, the persistent luminescent intensity of ZGGO:Ni phosphor upon the treatment of different ratio of $H_2O/D_2O$ (v/v) in Figure S9 (Supporting Information) further validates this specific response. Collectively, the above results indicate a selective responsiveness of NIR ZGGO:Ni phosphor to certain solvents. Given that all three molecules contain hydroxyl groups, it is reasonable to attribute the quenching of NIR II luminescence to the adsorption of these hydroxyl groups.[18]

Indeed, aside from solvents containing hydroxyl groups, it has been observed that solvents with carboxyl groups, such as formic acid (HCOOH), acetic acid ($CH_3COOH$), propionic acid ($CH_3CH_2COOH$) and n-caprylic acid ($C_8H_{16}O_2$), also effectively quench the NIR II persistent luminescence, as evidenced in Figure S10 (Supporting Information). The luminescent energy is likely transferred to specific environmental molecules,

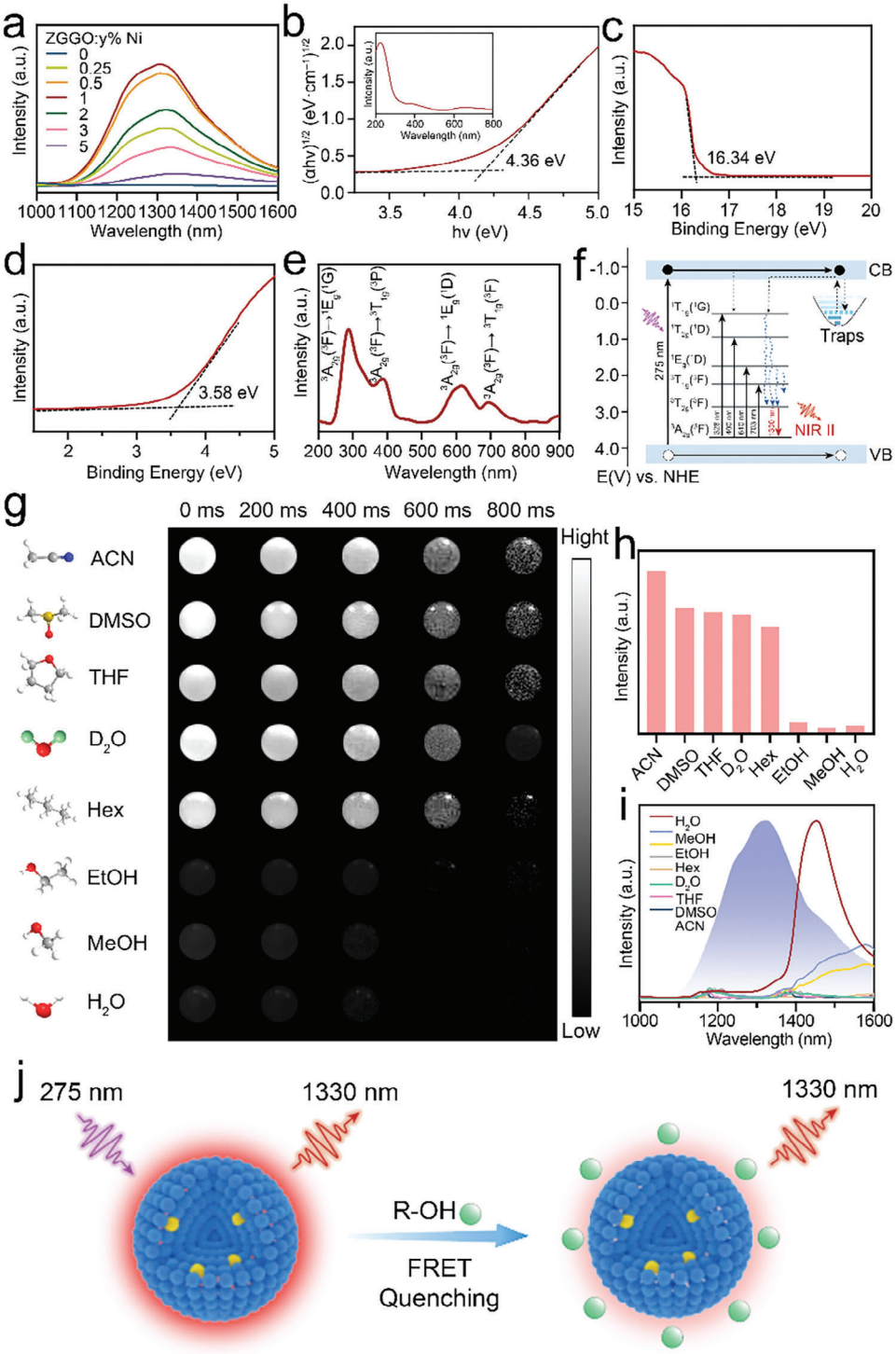


**Figure 2.** The NIR II luminescence mechanism and environmental response mechanism (a) Persistent luminescence spectra of ZGGO:Ni with different Ni content in NIR region. (b) Tauc plot of ZGGO:Ni. UPS spectrum of ZGGO:Ni to determine the corresponding (c) $E_{fermi}$ and (d) $E_{cutoff}$. (e) Excitation spectra of ZGGO:Ni. (f) Schematic illustration of the NIR II luminescence mechanism of ZGGO:Ni. (g) NIR persistent luminescence decay images upon the addition of different solvent across time. (h) NIR persistent luminescence intensity upon the addition of different solvent. (i) Emission spectra of ZGGO:Ni nanophosphors and absorption spectrum of different solvents. (j) Schematic illustration of the NIR II luminescence quenching mechanism of ZGGO:Ni.

leading to the evidently observed changes in luminescence. As depicted in the Fourier transform infrared spectra in Figure S11 (Supporting Information), the presence of both hydroxyl and amino groups on the surface of ZGGO:Ni nanophosphors is evident. The observed quenching of NIR II luminescence in solvents containing hydroxyl and carboxyl groups is likely attributed to the specific solvents' close adsorption and interaction to the nanophosphor surface and the subsequent fluorescence resonance energy transfer (FRET) mechanism. To further validate the above conjecture, absorption spectrum of various solvents were measured.[9g] As shown in Figure 2i, overlaps between the normalized NIR emission spectra of ZGGO:Ni nanophosphors with the absorption spectrum of solvents containing hydroxyl groups can be observed, indicating the occurrence of energy transfer from ZGGO:Ni nanophosphors to solvents. On the whole, according to the above results and considering that the energy transfer typically need to meet two key factors: distance and matched energy,[19] it is reasonable to attribute the quenching of NIR II luminescence to the intimate adsorption and interaction of specific solvents with ZGGO:Ni, followed by the subsequent fluorescence resonance energy transfer (FRET) mechanism (Figure 2j).

As demonstrated above, it is validated that the luminescence emission of $H_2O$/ZGGO:Ni solution is totally quenched. Thus, we argue that instead of undergoing a recombination process, photo-excited electrons from ZGGO:Ni are transferred to external substance $H_2O$.[20] The transferred photo-excited electrons might be promising for water-splitting. To test the speculation, both the hydrogen evolution reaction (HER) and the oxygen evolution reaction (OER) were further tested. Interestingly, it can be seen that the ZGGO:Ni nanophosphors achieve hydrogen evolution reaction with the rate of 613.66 μmol $h^{-1}$ $g^{-1}$ at 2 h as shown in Figure S12a (Supporting Information). This result is consistent with the band structure in which the CB edge potential of ZGGO:Ni locates at −0.40 V, more negative than the redox potential of $H^+/H_2$, that is energetically favorable for the hydrogen evolution reactions (Figure S12b) (Supporting Information). The above results indicate that our work might offer special insights for photocatalyst selection and design.

### 2.3. Reversible and Environment-Interactive Information Encryption

Equipped with the distinctive capabilities of environmental responsiveness and NIR II persistent luminescence, the prepared NIR II ZGGO:Ni nanophosphor has enabled us to devise a reversible and environment-interactive information encryption strategy featuring multichannel encoding as illustrated in **Figure 3**. Currently, a serious phosphors with different emission wavelengths based on ZGGO host have been reported. For example, ZGGO:Mn and ZGGO:Cr nanomaterals have the emissions ≈535 and 709 nm respectively (Figure S13, Supporting Information). In other words, the color tunability can be easily achieved by the different ion doping, which offers a multiple emission strategy for anticounterfeiting with high security level. The integration of the prepared multi-responsive and dynamic NIR II ZGGO:Ni nanophosphors with ZGGO:Mn and ZGGO:Cr has enabled the construction of multichannel encoding, thereby enhancing the anti-counterfeiting properties of the information.[5b,21] As shown in Figure 3a, the flower picture information is successfully encrypted and the accurate decryption of the encrypted information requires decoding at a specific wavelength after the cessation of specific excitation light irradiation under 275 nm (Figure S14, Supporting Information). Furthermore, considering that the NIR lifetimes of ZGGO:Ni nanophosphors can be regulated through doping with different concentration of $Ni^{2+}$, the information can be encrypted dynamically from the dimension of lifetime. As show in Figure 3b, the correct "3051" number information can be only decoded at a specific time after the excitation ceases (Figure S15, Supporting Information). Moreover, the dimension of environmental stimuli can provide an added layer of protection for information encryption. As demonstrated in Figure 3c, the "WHU" character exhibits dynamic and reversible responses to external stimuli such as temperature and humidity. Consequently, the information is only accessible under specific environmental conditions, further securing the encryption (Figure S16, Supporting Information).

Equipped with the versatile and dynamically responsive NIR II ZGGO:Ni nanophosphors, we have advanced to develop an innovative anti-counterfeiting strategy. This code-in-code strategy employs smart encoding across multiple dimensions, including wavelength, luminescence lifetime, and external stimuli such as temperature and humidity as illustrated in Figure 3d. Specifically, the encrypted information was encoded into a quick-response code, which can present various contents under different wavelengths, time frames, and environmental conditions. The accurate retrieval of the information is contingent upon accessing it at a precise condition, effectively filtering out and separating interfering data to access the intended message (Figures S17–S20, Supporting Information). Additionally, it merits emphasis that the prepared NIR II ZGGO:Ni nanophosphors have exhibited remarkable reversibility and stability, as evidenced by the XRD patterns and persistent luminescence spectrum in Figures S21 and S22 (Supporting Information). Overall, the multi-responsive NIR II persistent luminescent strategy presented in this study is anticipated to offer a straightforward approach for optimizing the optical properties of NIR II persistent luminescent materials. Furthermore, it is poised to open up avenues for expanding their applications in multi-dimensional and dynamic information encryption, thereby enhancing their utility in advanced security technologies.

## 3. Conclusion

In summary, this study successfully synthesized $Zn_{1.2}Ga_{1.6}Ge_{0.2}O_4$:$Ni^{2+}$ (ZGGO:Ni) nanophosphor with NIR II emission that is responsive to environmental stimuli, including temperature and solvent variations. It was observed that the NIR II persistent luminescence intensity was diminished in solvents containing hydroxyl groups, such as water ($H_2O$) and ethyl alcohol ($C_2H_6O$), while the persistent luminescence intensity was retained in solvents lacking hydroxyl groups, such as n-hexane ($C_6H_{14}$) and deuterated water ($D_2O$). The quenching effect, as evidenced by the outcomes and supported by prior research, can be reasonably ascribed to the specific solvents' close adsorption and interaction to the nanophosphor surface and the subsequent FRET mechanism. Furthermore, leveraging

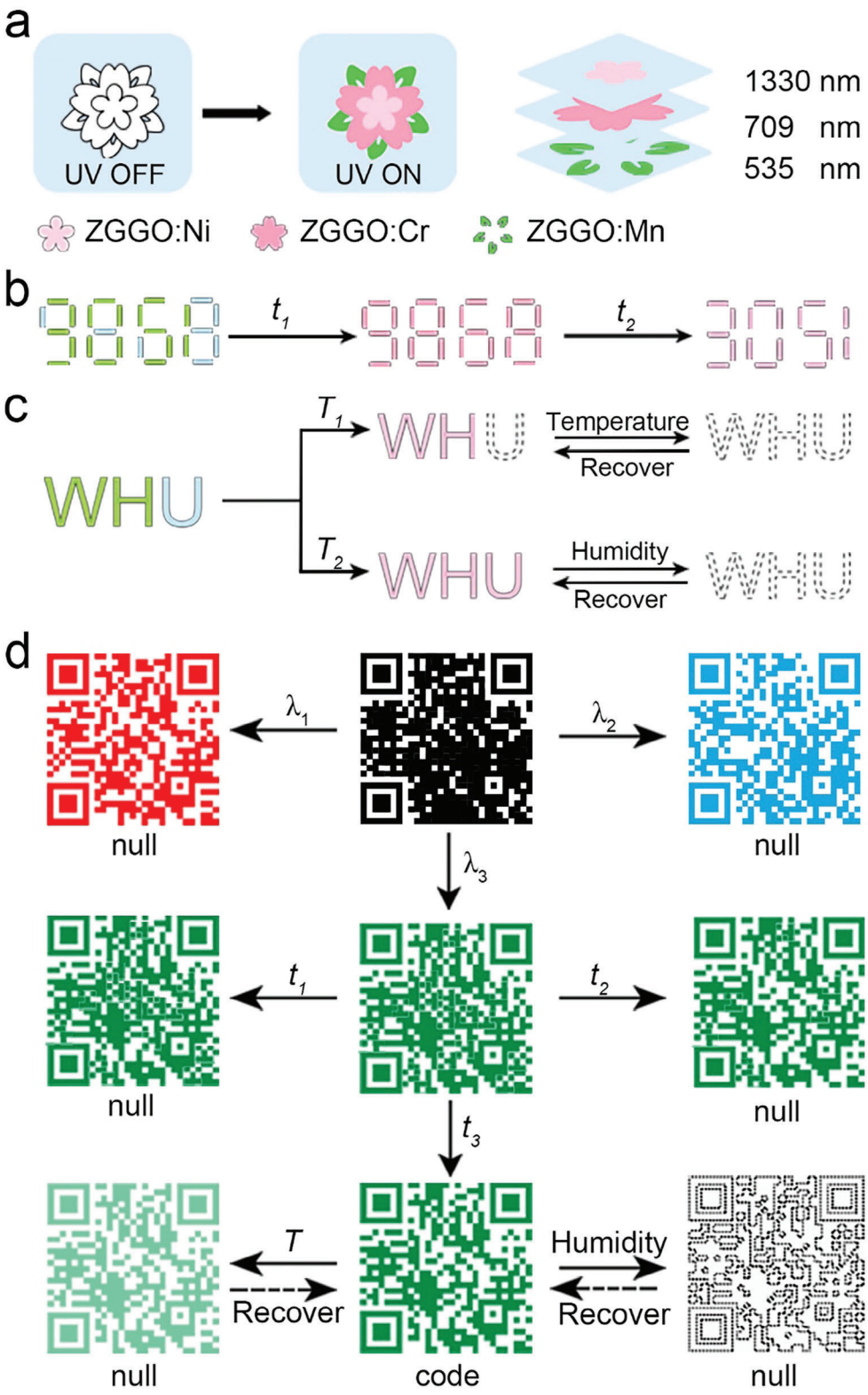


**Figure 3.** The application of NIR II ZGGO:Ni nanophosphors in multi-dimension and dynamic information encryption. (a) Encryption of picture based on ZGGO:Ni, ZGGO:Mn, and ZGGO:Cr with different emission wavelength. (b) Encryption of numbers based on NIR II ZGGO:Ni nanophosphors with different luminescence lifetime. (c) Encryption of characters based on environmental stimulus including temperature and humidity. (d) Implementation of controllable orthogonal encryption techniques by integrating ZGGO phosphors with the code-within-code strategy.

the versatile and dynamically responsive NIR II ZGGO:Ni nanophosphors, an innovative anti-counterfeiting strategy has been developed. This strategy allows for the encryption of information across multiple dimensions, including wavelength, luminescence lifetime and external stimuli like temperature and humidity, significantly enhancing information security. The multi-responsive NIR II phosphor strategy presented in this study is anticipated to provide a simplified method for optimizing the optical properties of NIR II nanophosphors and to pave pathways for their applications in multi-dimensional and environment-interactive information encryption, thereby reinforcing their role in cutting-edge security technologies.

## 4. Experimental Section

*Materials*: Nickel nitrate ($Ni(NO_3)_2{\cdot}9H_2O$), zinc nitrate hexahydrate ($Zn(NO_3)_2{\cdot}6H_2O$), sodium hydroxide (NaOH), ammonium hydroxide ($NH_3{\cdot}H_2O$), concentrated nitric acid ($HNO_3$), anhydrous ethanol, and sulfuric acid were procured from Sinopharm Chemical Reagent Co., Ltd. (China). Gallium nitrate ($Ga(NO_3)_3$) and germanium oxide ($GeO_2$) were sourced from Shanghai Maclin Biochemical Technology Co.

*Characterization*: The morphological features of the samples were examined using a transmission electron microscope (JEOL JEM-2100, Japan, 200 kV). The crystal structure of ZGGO:Ni was investigated with an X-ray powder diffraction system (Buerker D8 Advance, Germany) employing Cu-K$\alpha$ radiation (wavelength $\lambda = 1.5406$ Å). X-ray photoelectron spectroscopy (Thermo Fisher Scientific Escalab 250Xi) was utilized for the analysis of X-ray photoelectron spectra. The morphology and elemental composition of ZGGO:Ni were analyzed with a scanning electron microscope (Zeiss Merlin Compact) and energy-dispersive X-ray spectroscopy (Zeiss Merlin Compact, Germany). The persistent luminescence and excitation spectra, decay curves, and transient decay curves of the samples were recorded on a fluorescence spectrometer (Edinburgh Instruments FLS980). The ultraviolet/visible diffuse reflectance spectrum was obtained with a Shimadzu UV-3600 spectrometer. $Ni^{2+}$ doping contents were determined with inductively coupled plasma mass spectrometry (ICP-MS) (PQ-MS).

*Synthesis of the ZGGO:X% $Ni^{2+}$*: The 0.4 M $Na_2GeO_3$ solution was prepared by thoroughly reacting solid $GeO_2$ with an aqueous NaOH solution. Additionally, 0.5 M $Ga(NO_3)_3$, 0.5 M $Zn(NO_3)_2$, 0.4 M $Ga(NO_3)_3$, and 0.1 M $Ni(NO_3)_2$ solutions were prepared as precursor solutions for the synthesis of ZGGO:X% $Ni^{2+}$ nanoparticles.

The ZGGO:X% $Ni^{2+}$ nanoparticles were synthesized by a hydrothermal method. The preparation of ZGGO:1% $Ni^{2+}$ was used as an example. Briefly, 3.2 mL of $Ga(NO_3)_3$, 2.4 mL of $Zn(NO_3)_2$, 0.5 mL of $Na_2GeO_3$, and 0.5 mL of $Ni(NO_3)_2$ were sequentially added to a beaker according to the stoichiometric ratio. Then, an appropriate amount of $NH_3{\cdot}H_2O$ (28 wt.%) was added with magnetic stirring to adjust the pH of the solution to 8.5. Then the solution was stirred for 1 h at room temperature. After that, the solution was transferred into a Teflon-lined autoclave and reacted at 220 °C for 10 h. The resulting product was then obtained by centrifugation and washed with deionized water to obtain the prepared ZGGO:Ni nanoparticles. Following the above steps, the remaining ZGGO:X% $Ni^{2+}$ nanoparticles can be synthesized using corresponding amounts of $Ga(NO_3)_3$, $Zn(NO_3)_2$, $Na_2GeO_3$, and $Ni(NO_3)_2$ solutions.

*Valence Band Energy Calculation*: The valence band energy ($E_{VB}$), equivalent to the ionization potential, was assessed using ultraviolet photoelectron spectroscopy (UPS). With the formula $h\nu + E_{Fermi} - E_{cutoff}$ (where $h\nu$ is 21.22 eV, representing the excitation energy of the He I Source Gun), the $E_{VB}$ values for ZGGO:Ni can be calculated. Based on the vacuum energy ($E_{VB(vacuum)}$) and the normal hydrogen electrode potential ($E_{VB(NHE)}$), the $E_{VB}$ versus NHE values were determined. Combining this data with the bandgap values obtained from UV-vis diffuse reflectance spectra, the band positions of ZGGO:Ni were established.

The bandgap energy of the persistent photocatalyst, representing the energy needed to excite an electron from the valence band to the conduction band, was calculated using the Tauc plot method. This method, as described in previous studies, relies on the energy-dependent absorption coefficient $\alpha$, which can be expressed by the equation:

Where $h$ represents the Planck constant, $\nu$ represents the photo's frequency, E represents the bandgap and $c$ is a constant. The $r$ factor depends on the nature of the electron transition and is equal to 1/2 or 2 for the direct and indirect transition bandgaps respectively. Here, $r$ factor was set as 2 according to the previous reference. According to the Tauc plot, the bandgap of ZGGO:Ni were calculated.

*The measurement of ZGGO:Ni Persistent Luminescence Decay Image*: The NIR-II small animal InGaAs camera (NIR vana, Princeton Instruments) was utilized to characterize the persistent luminescence decay images of the samples. An optical filter is utilized to filter out wavelengths shorter than 1045 nm. 50 mg sample was loaded in a 96-well plate and pre-excited for 2 min by a ZF-5 portable ultraviolet lamp (16 W, $\lambda = 365$ nm). The exposure time for NIR-II fluorescence imaging was st at 200 ms.

*The Calculation of the Luminescence Lifetime of ZGGO:Ni*: The persistent luminescence decay curve of ZGGO:Ni was measured using a fluorescence spectrometer at room temperature. The excitation wavelength of 275 nm were used as the measurement condition. The resulting data was fitted with a third order-exponential decay model, expressed by the following formula.

$$I_{(t)} = A_1 e^{\left(\frac{-t}{\tau_1}\right)} + A_2 e^{\left(\frac{-t}{\tau_2}\right)} + I_0 \quad (1)$$

Among them, $I_{(t)}$ represents intensity, $\tau_1$, $\tau_2$, and $\tau_3$ were the persistent luminescence decay lifetime of the fast and slow components, respectively. $A_1$, $A_2$, and $A_3$ denoted the amplitudes at t = 0, and $I_0$ was a constant. The persistent luminescence decay lifetime $\tau$ can be calculated from the decay lifetimes and amplitudes corresponding to these two components:

$$\tau = \frac{A_1\tau_{\tau_1}^2 + A_1\tau_{\tau_1}^2}{A_1\tau_1 + A_2\tau_2} \quad (2)$$

*Trap Depth Analysis*: Trap depth $E$ can be approximated by Urbach method:

$$E = \frac{T_m}{500} \quad (3)$$

where $T_m$ represents the temperature corresponding to the luminescence peaks. According to previous reports, the trap ranging from 0.6 to 0.7 eV can easily release captured electrons at room temperature. Conversely, deeper traps require extrinsic stimulation (such as heat or optical treatment) to facilitate electron release.

*Photocatalytic $H_2$ Evolution Tests*: The photocatalytic activity of ZGGO:Ni for hydrogen evolution was evaluated in a sealed Pyrex glass irradiation system. To begin, a platinum (Pt) co-catalyst was deposited in situ onto the ZGGO:Ni support, with an intended Pt loading of 1 wt%. Specifically, 200 mg of ZGGO:Ni photocatalyst powder was dispersed in a 60 mL methanol solution with a volume fraction of 33%, containing $H_2PtCl_6$ at a concentration of 0.2 mmol $L^{-1}$. After 30 min of ultrasonic dispersion, the in situ photodeposition of Pt was carried out using a 500 W mercury lamp for 3 h. Post-Pt deposition, the modified photocatalyst was placed into the reaction setup and vacuum was applied. The system was then exposed to simulated solar irradiation using a xenon lamp (PLS-SXE300/300UV, PerfectLight, Beijing, China) to assess the photocatalytic performance. The gases produced in the reaction vessel were collected with a microinjector pump and analyzed by gas chromatography (GC-14C, Shimadzu, Japan).

## Supporting Information

Supporting Information is available from the Wiley Online Library or from the author.

## Acknowledgements

This work is supported by the National Natural Science Foundation of China (21925401, 52221001 to Q.Y.), the National Key R&D Program of China (2023YFF1205900 to Q.Y.), the Fundamental Research Funds for the Central Universities (2042022rc0004 to Q.Y), Hunan Provincial Key Research and Development Plan (2024JK2117 to Q.Y.), "Sharp Knife" Technology Research Program of Hubei Province (2023BAA002 to Q.Y), China Postdoctoral Science Foundation (2024M752456 to C.N), Postdoctoral Innovative Research of Hubei Province of China (211000025 to C.N), Youth Talent Program of Sci-Tech Think Tank (XMSB20240710060 to C.N), New Cornerstone Science Foundation through the XPLORER PRIZE, Interdisciplinary Innovative Talents Foundation from Renmin Hospital of Wuhan University. The authors thank the Core Facility of Wuhan University for TEM and ICP-MS.

## Conflict of Interest

The authors declare no conflict of interest.

## Data Availability Statement

The data that support the findings of this study are available in the supplementary material of this article.

## Keywords

fluorescence resonance energy transfer, information encryption, multiple responses, NIR II Nanophosphors, ZGGO:Ni

Received: October 26, 2024
Revised: December 2, 2024
Published online:

[1] a) X. Li, J. Liu, D. Li, S. Huang, K. Huang, X. Zhang, *Adv. Sci.* **2021**, *8*, 2101295; b) S. Zeng, K. Shen, S. Li, R. Li, Z. Hou, X. Zhang, W. R. T. Tait, T. Kajiwara, A. Takahara, A. T. Smith, M. D. Jones, D. Zhang, L. Sun, *Adv. Funct. Mater.* **2021**, *31*, 2100612; c) R. Wang, Y. Zhang, W. Lu, B. Wu, S. Wei, S. Wu, W. Wang, T. Chen, *Angew. Chem. Int. Ed.* **2023**, *62*, 202300417.

[2] a) Y. Sun, Y. Wang, Y. Liu, S. Wu, S. Zhang, W. Niu, *Adv. Funct. Mater.* **2022**, *32*, 2204467; b) Y. Wu, Y. Wang, S. Zhang, S. Wu, *ACS Nano* **2021**, *15*, 15720.

[3] a) H. Han, J. W. Oh, H. Lee, S. Lee, S. Mun, S. Jeon, D. Kim, J. Jang, W. Jiang, T. Kim, B. Jeong, J. Kim, D. Y. Ryu, C. Park, *Adv. Mater.* **2024**, *36*, 2310130; b) H. Wang, Y. Tang, Z. Huang, F. Wang, P. Qiu, X. Zhang, C. Li, Q. Li, *Angew. Chem. Int. Ed.* **2023**, *62*, 202313728; c) J. Yin, X. Huo, X. Cao, R. Li, Y. Zhou, T. Jiang, L. Wang, Z. Wu, Z. L. Wang, *ACS. Mater. Lett.* **2023**, *5*, 11; d) Z. Li, Y. Yin, *Adv. Mater.* **2019**, *31*, 1807061.

[4] D. Li, J. Wu, Z. Liang, L. Li, X. Dong, S. Chen, T. Fu, X. Wang, Y. Wang, F. Song, *Adv. Sci.* **2022**, *10*, 2206290.

[5] X. Chen, C. X. Hu, Y. Wang, T. Li, J. Jiang, J. Huang, S. B. Wang, W. F. Dong, J. L. Qiao, *Adv. Sci.* **2024**, *11*, 2304946.

[6] J. Li, X. Huang, X. Zhao, L. J. Chen, X. P. Yan, *Angew. Chem. Int. Ed.* **2020**, *60*, 2398.

[7] a) N. Chen, N. Du, W. Wang, T. Liu, Q. Yuan, Y. Yang, *Angew. Chem. Int. Ed.* **2022**, *61*, 202115572; b) N. Chen, N. Du, R. Shen, T. He, J. Xi, J. Tan, G. Bian, Y. Yang, T. Liu, W. Tan, L. Yu, Q. Yuan, *Nat. Commun.* **2023**, *14*, 6800; c) R. Shen, T. He, S. Yao, Y. Zhang, T. Peng, W. Tan, N. Chen, Q. Yuan, *Small Methods* **2024**, 2400439; d) N. Chen, X. Zhang, J. Xi, Y. Yang, Q. Yuan, *Sci. China. Chem.* **2023**, *66*, 2941; e) N. Chen, D. Cheng, T. He, Q. Yuan, *Chinese. J. Chem.* **2023**, *41*, 1836; f) Y. Wang, K. Jiang, J. Du, L. Zheng, Y. Li, Z. Li, H. Lin, *Nano-Micro. Lett.* **2021**, *13*, 198.

[8] a) Y. Zhang, L. Chen, B. Liu, S. Yu, Y. Yang, X. Liu, *Adv. Funct. Mater.* **2024**, *34*, 2315366; b) Y. Yang, Z. Li, J. Zhang, Y. Lu, S. Guo, Q. Zhao, X. Wang, Z. Yong, H. Li, J. Ma, Y. Kuroiwa, C. Moriyoshi, L. Hu, L. Zhang, L. Zheng, H. Sun, *Light-Sci. Appl.* **2018**, *7*, 88; c) Y. Zhang, R. Huang, H. L. Li, Z. X. Lin, D. J. Hou, Y. Q. Guo, J. Song, C. Song, Z. Lin, W. X. Zhang, J. Wang, P. K. Chu, C. Zhu, *Small* **2020**, *16*, 2003121.

[9] a) L. Chen, K. Sun, D. Hu, X. Su, L. Guo, J. Yin, Y. Pei, Y. Fan, Q. Liu, M. Xu, W. Feng, F. Li, *Angew. Chem. Int. Ed.* **2023**, *62*, 202218670; b) Y. Li, J. Sun, M. Chen, S. Miao, M. Liu, Y. Ma, G. Wang, X. Gu, B. Z. Tang, *Adv. Funct. Mater.* **2022**, *32*, 2205494; c) Q. Li, D. Cheng, H. Gu, D. Yang, Y. Li, S. Meng, Y. Zhao, Z. Tang, Y. Zhang, J. Tan, S. Qu, *Chem. Eng. J.* **2023**, *462*, 142339; d) X. Wang, J. Du, H. Lin, *Small Methods* **2023**, *8*, 2301001; e) Q. Li, Y. Huang, H. Zhu, Y. Zhu, Y. Yi, X. Li, H. Chen, B. Li, D. Li, Y. Chang, *Adv. Sci.* **2024**, *11*, 2408097; f) M. Chan, Y. Chang, *Anal. Bioanal. Chem.* **2024**, *416*, 3887; g) S. F. Wang, Y. Fan, D. Li, C. X. Sun, Z. H. Lei, L. F. Lu, T. Wang, F. Zhang, *Nat. Commun.* **2019**, *10*, 1058; h) Y. Chen, S. F. Wang, F. Zhang, *Nat. Rev. Bioeng.* **2023**, *1*, 60; i) H. H. Liu, F. Ren, H. Zhang, Y. B. Han, H. Z. Qin, J. F. Zeng, Y. Wang, Q. Sun, Z. Li, M. Y. Gao, *J. Mater. Chem. B.* **2018**, *6*, 1508;

[10] a) P. Pei, Y. Chen, C. X. Sun, Y. Fan, Y. M. Yang, X. Liu, L. F. Lu, M. Y. Zhao, H. X. Zhang, D. Y. Zhao, X. G. Liu, F. Zhang, *Nat. Nanotechnol.* **2021**, *16*, 1011; b) X. Li, X. Y. Shen, M. Lu, J. L. Wu, Y. Zhong, Z. N. Wu, W. W. Yu, Y. B. Gao, J. H. Hu, J. Y. Zhu, Y. Zhang, X. Bai, *Angew. Chem. Int. Ed.* **2023**, *62*, 202217832; c) X. Z. Chen, Y. Li, K. Huang, L. Huang, X. M. Tian, H. F. Dong, R. Kang, Y. H. Hu, J. M. Nie, J. R. Qiu, G. Han, *Adv. Mater.* **2021**, *33*, 2008722; d) S. H. Zheng, J. P. Shi, X. Y. Fu, C. C. Wang, X. Sun, C. J. Chen, Y. X. Zhuang, X. Y. Zou, Y. C. Li, H. W. Zhang, *Nanoscale* **2020**, *12*, 14037; e) Y. Q. Liu, J. K. Li, J. Q. Xiahou, Z. M. Liu, *J. Fluoresc.* **2023**, https://doi.org/10.1007/s10895-023-03513-8.

[11] a) J. Wang, Q. Ma, X. Hu, H. Liu, W. Zheng, X. Chen, Q. Yuan, W. Tan, *ACS Nano* **2017**, *11*, 8010; b) X. Lv, N. Chen, J. Wang, Q. Yuan, *Sci. China. Mater.* **2020**, *63*, 1808; c) J. Wang, Q. Ma, W. Zheng, H. Liu, C. Yin, F. Wang, X. Chen, Q. Yuan, W. Tan, *ACS Nano* **2017**, *11*, 8185; d) Y. J. Li, X. P. Yan, *Nanoscale* **2016**, *8*, 14965;

[12] a) A. Satpathy, W. T. Huang, M. H. Chan, T. Y. Su, M. Kamiński, N. Majewska, S. Mahlik, G. Leniec, S. M. Kaczmarek, M. Hsiao, R. S. Liu, *Adv. Opt. Mater.* **2023**, *11*, 2300321. b) J. K. Lyu, B. Dong, G. C. Pan, L. H. Sun, X. Bai, S. T. Hu, B. Shen, B. S. Zhou, L. Wang, W. Xu, D. L. Zhou, L. Xu, H. W. Song, *Nanoscale* **2021**, *13*, 16598.

[13] a) L. F. Yuan, Y. H. Jin, H. Y. Wu, K. Y. Deng, B. Y. Qu, L. Chen, Y. H. Hu, R. S. Liu, *ACS Appl. Mater. Interfaces.* **2022**, *14*, 4265; b) Y. Zhang, Z. X. Gao, Y. Y. Li, H. P. Wang, S. L. Zhao, Y. Shen, D. G. Deng, S. Q. Xu, H. Yu, *ACS Appl. Mater. Interfaces.* **2024**, *16*, 57316; c) V. Rajendran, W. T. Huang, K. C. Chen, D. H. Wei, H. Chang, R. S. Liu, *ACS Appl. Opt. Mater.* **2023**, *1*, 1063; d) D. J. Liu, G. G. Li, P. P. Dang, Q. Q. Zhang, Y. Wei, L. Qiu, H. Z. Lian, M. M. Shang, J. Lin, *Light. Sci. Appl.* **2023**, *12*,248.

[14] a) A. Satpathy, W. Huang, M. H. Chan, T. Y. Su, M. Kaminski, N. Majewska, S. Mahlik, G. Leniec, S. M. Kaczmarek, M. Hsiao, R. S. Liu, *Adv. Opt. Mater.* **2023**, *11*, 2300321; b) W. T. Huang, V. Rajendran, M. H. Chan, M. Hsiao, H. Chang, R. S. Liu, *Adv. Opt. Mater.* **2023**, *11*, 2202061.

[15] Y. Ding, C. Yang, F. Gan, G. Zhang, C. Shen, H. Qiu, *J. Am. Chem. Soc.* **2024**, *146*, 25211.

[16] N. J. J. Johnson, S. He, S. Diao, E. M. Chan, H. Dai, A. Almutairi, *J. Am. Chem. Soc.* **2017**, *139*, 3275.
[17] Y. Zhu, J. Yang, Y. Meng, M. Wang, H. Zhu, D. Yan, C. Liu, C. Xu, Y. Liu, *J. Am. Ceram. Soc.* **2022**, *106*, 1203.
[18] a) S. Faulkner, S. J. A. Pope, B. P. Burton-Pye, *Appl. Spectrosc. Rev.* **2005**, *40*, 1; b) J. Maillard, K. Klehs, C. Rumble, E. Vauthey, M. Heilemann, A. Fürstenberg, *Chem. Sci.* **2021**, *12*, 1352; c) J. Kucera, P. Lubal, S. Lis, P. Taborsky, *Talanta* **2018**, *184*, 364.
[19] a) G. Agam, C. Gebhardt, M. Popara, A. Barth, C. A. M. Seidel, D. C. Lamb, T. Cordes, *Nat. Methods* **2023**, *20*, 523; b) Y. J. Zuo, Z. M. Gou, Y. Lan, M. Yan, *Trends Analt. Chem.* **2023**, *167*, 117271.
[20] H. Zhang, H. Liu, Z. Q. Tian, D. Lu, Y. Yu, S. Cestellos-Blanco, K. K. Sakimoto, P. D. Yang, *Nat. Nanotechnol.* **2018**, *13*, 900.
[21] X. Zhang, X. Hou, J. Gao, Z. Wang, X. Zhao, C. Xu, D. Gao, *J. Mater. Chem. C.* **2023**, *11*, 16631.